



**HAL**  
open science

## Structure-activity relationship study: Mechanism of cyto-genotoxicity of Nitropyrazole-derived high energy density materials family

Laetitia Guyot, Florian Simon, Jessica Garcia, Floriane Vanhalle, Gaelle Vilchez, Claire Bardel, Brigitte Manship, Alain Puisieux, Christelle Machon, Guy Jacob, et al.

### ► To cite this version:

Laetitia Guyot, Florian Simon, Jessica Garcia, Floriane Vanhalle, Gaelle Vilchez, et al.. Structure-activity relationship study: Mechanism of cyto-genotoxicity of Nitropyrazole-derived high energy density materials family. *Toxicology and Applied Pharmacology*, 2019, 381, pp.114712 -. 10.1016/j.taap.2019.114712 . hal-03487645

**HAL Id: hal-03487645**

**<https://hal.science/hal-03487645>**

Submitted on 20 Dec 2021

**HAL** is a multi-disciplinary open access archive for the deposit and dissemination of scientific research documents, whether they are published or not. The documents may come from teaching and research institutions in France or abroad, or from public or private research centers.

L'archive ouverte pluridisciplinaire **HAL**, est destinée au dépôt et à la diffusion de documents scientifiques de niveau recherche, publiés ou non, émanant des établissements d'enseignement et de recherche français ou étrangers, des laboratoires publics ou privés.



Distributed under a Creative Commons Attribution - NonCommercial 4.0 International License

1           **Structure-activity relationship study: mechanism of cyto-**  
2           **genotoxicity of Nitropyrazole-derived high energy density**  
3           **materials family**

4  
5  
6   **Laetitia Guyot<sup>1,2</sup> Florian Simon<sup>1</sup> Jessica Garcia<sup>1</sup> Floriane Vanhalle<sup>1</sup> Gaelle Vilchez<sup>1</sup> Claire**  
7   **Bardel<sup>1</sup> Brigitte Manship<sup>2</sup> Alain Puisieux<sup>2,3</sup> Christelle Machon<sup>1</sup> Guy Jacob<sup>4,5</sup> Jérôme Guitton<sup>1,3,\*</sup>**  
8   **Léa Payen<sup>1,2,3</sup>**

9  
10   <sup>1</sup> Hospices Civils de Lyon, Centre Hospitalier Lyon-Sud, Laboratoire de biochimie-toxicologie,  
11   France.

12   <sup>2</sup> UMR INSERM U1052/CNRS 5286, Centre de Recherche en Cancérologie de Lyon, Centre Léon  
13   Bérard, France.

14   <sup>3</sup> Université Lyon 1, ISPBL, Faculté de pharmacie, Laboratoire de Toxicologie, France.

15   <sup>4</sup> Université Lyon 1, Faculté des sciences et technologies, UMR CNRS 5278 Hydrazines et Composés  
16   Energetiques Polyazotés, France.

17   <sup>5</sup> ArianeGroup Centre de Recherche du Bouchet, France

18  
19   \* To whom correspondence should be addressed: Pr. J. Guitton, Université Lyon 1, ISPBL, Faculté de  
20   pharmacie, Laboratoire de Toxicologie, 8 avenue Rockefeller, 69373, Lyon, France.

21   E-mail: [jerome.guitton@univ-lyon1.fr](mailto:jerome.guitton@univ-lyon1.fr)

22

## 23 **Abstract**

24 Stringent toxicological tests have to be performed prior to the industrial development of alternative chemicals particularly  
25 high energy dense materials (HEDMs) such as explosives. The properties (e.g., power, stability) of these compounds are  
26 constantly being improved, the current axis of research being the nitration of nitrogen heterocycles leading to HEDMs such  
27 as nitropyrazole-derived molecules. However, except for 3,4,5-trinitropyrazole (3,4,5-TNP), which was shown to be highly  
28 toxic in mice, the toxicological impact of these HEDMs has so far not been investigated. Furthermore, as industrials are  
29 strongly advised to develop alternative safety testing assays to *in vivo* experiments, we herein focused on determining the  
30 cytotoxic and genotoxic effects of seven Nitropyrazole-derived HEDMs on three rodent cell lines (mouse embryonic  
31 BALB/3T3 clone A31 cells, Chinese hamster ovary cells CHO-K1 and mouse lymphoma L5178Y TK +/- clone (3.7.2C)  
32 cells), two human fibroblast lines (CRC05, PFS04062) and on the human hepatic HepaRG model (both in proliferative and  
33 differentiated cells). A stronger cytotoxic effect was observed for 1,3-dinitropyrazole (1, 3-DNP) and 3,4,5-TNP in all cell  
34 lines, though differentiated HepaRG cells clearly displayed fewer likely due to the metabolism and elimination of these  
35 molecules by their functional biotransformation pathways. At the mechanistic level, the sub-chronic cytotoxic and  
36 genotoxic effects were linked to ROS/RNS production (experimental assays), HA2.X and to transcriptomic data  
37 highlighting the increase in DNA repair mechanisms.

38

39

## 40 **Keywords**

41 Nitropyrazole-derived; HEDMs; RNAseq; Genotoxicity

42

43

## 44 **Highlights**

45 \* A difference in cytotoxicity (until 200 fold) is observed between the nitropyrazoles

46 \* The impact on the cell cycle depends on the compounds

47 \* Oxidative stress pathways may be involved in the cellular cytotoxicity

48 \* Targeted metabolomics approach shown few modifications in endogenous metabolites

49

## 50 Introduction

51 Chemical explosives are highly reactive compounds that contain both their own oxygen (reaction initiator) and fuel  
52 (explosive compound) within the same molecule. Several parameters are important to the development of chemical  
53 explosives for military and civilian (e.g., building industry) applications, including a positive oxygen balance (i.e., a better  
54 detonator), a high enthalpy of formation (i.e., a better transfer of energy during the production of new molecules), a low  
55 sensitivity (offers better stability), a high stability (thermal and chemical) and a low level of toxicity. The initial inclusion  
56 of nitro functional groups (-NO<sub>2</sub>) to well-known liquid combustibles prior to World War I (WWI) gave rise to highly  
57 explosive molecules such as trinitrophenol or trinitrotoluene (TNT), while the consecutive addition of this functional group  
58 to the aromatic ring of such energetic molecules generated even more powerful compounds like 1,3,5-trinitro-1,3,5-  
59 triazinane (RDX) or 1,3,5,7-tetranitro-1,3,5,7-tetrazocane (HMX), used during WWII. However, owing to their instability,  
60 industrials introduced hydrogen-bound amino groups to nitro-based explosives to reduce their sensitivity, as exemplified  
61 in nitrotriazolone (NTO), 1,3,5-triamino-2,4,6-trinitrobenzene (TATB), and 1,1-diamino-2,2-dinitroethylene (FOX7). This  
62 unfortunately affected their energetic performance, and the current axis of research into improving the balance between  
63 energy and stability/sensitivity in high energy density materials (HEDMs) (Dalinger, 2010), is the nitration (addition of  
64 energetic -NO<sub>2</sub> groups) of nitrogen heterocycles, such as in the formation of nitropyrazole-derived molecules.

65 More and more studies are investigating the environmental toxicity of HEDMs. Nevertheless, little is known about the  
66 human toxicology and USEPA organization has recommended restrictions for lifetime contact through drinking water  
67 (Chatterjee *et al.*, 2017). For example to limit human exposition, laboratories are developing new transgenic western  
68 wheatgrass that degrades the explosive RDX and detoxifies TNT especially on live-fire training ranges, threatens  
69 environmental and human health (Zhang *et al.*, 2019). Recently, very interestingly, mixture effects of the insensitive  
70 munitions formulations IMX-101 (mixture of 2,4-dinitroanisole [DNAN], 3-nitro-1,2,4-triazol-5-one [NTO], and  
71 nitroguanidine [NQ]) and IMX-104 (DNAN, NTO, and RDX] were evaluated in subchronic and chronic water-only assays  
72 in *Hyalella azteca* assessing impacts on survival, growth and reproduction. Longer exposure duration to IMX-101, IMX-  
73 104, and DNAN resulted in higher sensitivity for lethality and decreased reproduction function (Lotufo *et al.*, 2018).  
74 Recently, to decipher toxicogenomic responses for the individual constituents of IMX-101, transcriptomic analysis were  
75 conducted. It was found that transcriptional regulations and functional responses characteristic of: oxidative stress,  
76 impaired energy metabolism, tissue damage and inflammatory responses in DNAN exposures; impaired steroid  
77 biosynthesis and developmental cell-signaling in NQ exposures; and altered mitogen-activated protein kinase signaling in  
78 NTO exposures (Gust *et al.*, 2018). Finally, for a molecular characterization of the RDX induced neurotoxicity, a  
79 transcriptomic analysis was conducted in RDX exposed rats. They observed an induction of miRNAs expression levels by

80 RDX. This could reduce the expression levels of POLE4, C5ORF13, SULF1 and ROCK2 genes. RDX regulated immune  
81 and inflammation response miRNAs and genes could contribute to RDX- induced neurotoxicity and other toxicities as well  
82 as animal defending reaction response to RDX exposure (Deng *et al.*, 2014). Taken altogether, new methodologies unable  
83 researchers to decipher the toxicological molecular mechanisms of these explosive molecules.

84 For the purpose of our study, these include the previously studied 3,4,5-trinitropyrazole (3,4,5-TNP) by our own group  
85 (Guyot *et al.* 2018), and its precursors or derivatives: 1-nitropyrazole (1-NP), 3-nitropyrazole (3-NP), 1,3-dinitropyrazole  
86 (1,3-DNP), 3,5-dinitropyrazole (3,5-DNP), 4-nitropyrazole (4-NP), and 1-methyl 4-nitropyrazole (1-Met-4-NP).  
87 Nevertheless, excluding our own *in vivo* toxicity and pharmacokinetic evaluation of 3,4,5-TNP (Guyot *et al.* 2018), few  
88 toxicological data are available for this family of pyrazole derivatives.

89 Here, based both on classical OECD Testing of Chemicals Guidelines, and on previously developed human cell line  
90 models, we evaluated (i) the *in vitro* toxicological impact and (ii) mechanisms of toxicity using a transcriptomic  
91 methodology of these nitropyrazole-derived HEDMs. Indeed, a high level of cytotoxicity and genotoxicity may be a go/no  
92 go decision in the development of a new industrial molecule, and consequently the toxic risk for humans has to be evaluated  
93 following strict methods (OECD - Guidelines for the Testing of Chemicals, Section 4). In this field, various functional  
94 assays and various animal models are used including murine embryonic BALB/3T3 clone A31 cells, Chinese hamster  
95 ovary cells CHO-K1 and mouse lymphoma L5178Y TK +/- clone (3.7.2C) cells.

96 Furthermore, owing to the most common route of entry (inhalation/skin contact) and most common toxic side effects  
97 (hepatotoxicity; owing to its role in the biotransformation of xenobiotics) for explosive molecule developers and civilians  
98 alike, the molecules were tested in two human fibroblast cell lines and in a human hepatic cell line, namely HepaRG. These  
99 hepatic cells are the first model of human cells able to differentiate *in vitro* into mature hepatocyte-like cells, while  
100 conserving major biotransformation functions including CYP3A4 metabolism, phase 2 enzymes, transporters and  
101 regulatory transcriptional factors (Aninat *et al.* 2006; Anthérieu *et al.* 2012; Le Vee *et al.* 2013). This cell line is successfully  
102 used in toxicological studies using toxigenomics and metabolomics methodology in differentiated state or spheroid state  
103 (Van den Eede *et al.*, 2015; Bell *et al.*, 2017; Moedas *et al.*, 2017; Limonciel *et al.*, 2018; Mesnage *et al.*, 2018; Ramaiahgari  
104 *et al.*, 2019). In this work, we identified 1,3-DNP and 3,4,5-TNP as the most cytotoxic molecules, and demonstrated that  
105 toxicological and cellular effects can be globally screened using the presented transcriptomic approaches, which enabled  
106 us to gain in objectivity with regards to the toxicological impact of exposure to xenobiotics (e.g., cellular pathway  
107 dysregulations).

## 108 **Materials and methods**

109

110 **Reagents and chemicals**

111 Nitropyrazole-derived HEDMs were synthesized at the ArianeGroup research center (Hervé, 2007). The route involves  
112 several steps of N-Nitration and transposition of NO<sub>2</sub> ending by a mixed acids nitration on the carbon atom in the 4 position.  
113 These molecules were obtained either in pure water (3,4,5-TNP at 1M), in dimethyl sulfoxide (DMSO; 1,3-DNP at 100  
114 mM and 3-NP at 1 M) or into acetonitrile (ACN; 1-NP, , 4-NP and 1-Met-4-NP at 1M and 3,5-DNP at 770 mM; Table 1);  
115 the initial choice of solvent depending on their physicochemical properties. Nitropyrazole-derived HEDMs were stored at  
116 4°C in the dark under a slight nitrogen stream. Doxorubicin, DMSO, ammonium sulfate, and ACN (HPLC grade) were  
117 purchased from Sigma-Aldrich (Saint-Quentin Fallavier, France). Acetic acid (Ultra-pure, > 99.5%) and ammonia (30%)  
118 were purchased from Carlo Erba reagents (Milano, Italy). Milli-Q deionized water was used throughout the study. Drug-  
119 free normal plasma was provided by the regional blood bank (EFS Rhône-Alpes, France).

120

121 **Tissue culture**

122 L5178Y TK +/- clone (3.7.2C), CHO-K1 (ATCC® CCL61™), and BALB/3T3 clone A31 (ATCC® CCL163™) cells were  
123 purchased from the ATCC biological resources center (<https://www.lgcstandards-atcc.org>). The tissue culture conditions  
124 strictly followed guidelines provided by the ATCC. HepaRG cells were purchased from Biopredic International (Rennes,  
125 France) and cultured according to their guidelines. Two primary human normal fibroblast cell lines, PSF04062 and CRC05,  
126 were cultured in DMEM (Dulbecco's Modified Eagle Medium, Life Technologies (#31966047)) supplemented with 10%  
127 FCS, 100 units/ml penicillin, 100 µg/ml streptomycin, and 2 mM glutamine.

128

129 **Cytotoxicity and cell proliferation assays**

130 To evaluate the cytotoxicity of nitropyrazole-derived molecules, two methods were applied, namely, the MTT assay to  
131 assess cell viability and the xCELLigence technique for a dynamic monitoring of cell viability and proliferation. Briefly,  
132 for the MTT assay, cells were seeded onto 96-well culture plates at a density of 1,000-8,000 cells/well (according to the  
133 rate of proliferation of the studied cell line). The cells were exposed to Nitropyrazole-derived HEDMs (at a final  
134 concentration ranging from 0.0016 mM to 10 mM) for 72 h, and cell viability/growth/proliferation was then assessed by  
135 applying MTT (3-(4,5-dimethylthiazol-2-yl)-2,5-diphenyltetrazolium bromide) to the cells. Formazan production was  
136 measured spectrophotometrically at OD = 550 nm (MultiSkanAscent, ThermoFisher Scientific™ #51118407). The  
137 following formula was used to determine the IC<sub>50</sub> (%) (inhibitory concentration) = ((OD of the sample - OD of the  
138 control)/(OD of the control))x100. For each condition four technical and at least three independent biological  
139 measurements were obtained.

140 The xCELLigence system (ACEA Biosciences, San Diego, CA, USA) was used following the manufacturer's protocol. In  
141 this system, 2000-5000 cells are grown in special chambers where they adhere to gold-coated microelectrodes that measure  
142 the relative change in electrode impedance, expressed as a cell index (CI), a unit less parameter, as a function of time. This  
143 measurement provides dynamic information on the number of cells attached/proliferating. Cells were then either treated  
144 with various concentrations of Nitroprazole-derived HEDMs or similar amounts of vehicle. The CI value of each group  
145 was monitored for 5 days. Each condition was duplicated, and at least three independent experiments were carried out.

146

#### 147 **RNA expression and quantitative real time PCR (RT-PCR) assays**

148 Total RNA was extracted and purified using the RNeasy Mini Kit (Qiagen # 74106). Amounts of RNA isolated from  
149 samples can vary due to the developmental stage, species, and growth conditions of the original sample. Furthermore, the  
150 RNeasy procedure enriches RNA species >200 nt and excludes 5S rRNA, tRNAs, or other low molecular weight RNAs.  
151 RNA was isolated on the silica membrane in trusted RNeasy spin columns, with binding capacities of 100 µg of RNA,  
152 according to the supplier's recommendations (Qiagen). The expression levels of various genes were quantified by PCR  
153 using the BIORAD CFX96 Touch™ (BIORAD, #1855195). The reverse transcription was carried out using Maxima First  
154 Strand cDNA Synthesis Kit (ThermoFisher #K-1642).

155

#### 156 **mRNA library preparation for next generation sequencing (NGS)**

157 For the preparation of the NGS RNA library, RNA concentration was measured using the GE NanoView  
158 Spectrophotometer (Biochrom US, Holliston, MA, US). The quality of RNA samples was analyzed using the RNA 6000  
159 Pico Kit running on the 2100 BioAnalyzer (Agilent Santa Clara, California, US). Total RNA samples were diluted to 20  
160 ng/µL in a final volume of 50 µL for a total input of 1 µg. Only the RNA pools with a RIN score higher than 9 were used  
161 in the NGS library preparation prior to sequencing. Firstly, mRNAs were isolated using the NEBNext Poly(A) mRNA  
162 Magnetic Isolation Module from 1 µg of total RNA. The isolation procedure is based on the selection of mRNA using  
163 oligo dT beads directed against polyA tails of intact mRNA. Secondly, the NGS libraries were created from mRNA isolated  
164 using the NEBNext Ultra II Directional RNA Library Prep Kit for Illumina (NewEngland BioLabs, Ipswich,  
165 Massachusetts). The sequencing reads were obtained after demultiplexing the raw sequencing data using bcl2fastq  
166 v2.19.1.403 (Version v2.15.0 for NextSeq™ 500 and HiSeq® X Systems, Illumina). After validating the quality controls  
167 of each sample using the FastQC v0.11.5 software (<https://www.bioinformatics.babraham.ac.uk/projects/fastqc/>). The  
168 alignment files were generated with STAR v2.5.2b (University of Birmingham) in the 2-pass mode. We used the hg19  
169 human genome as reference. This mode is known to improve the detection of more reads mapping novel splice junctions.

170 Once the final sorted alignment file was obtained, the count of reads was done with the GFOLD V1.1.4 (option – count;  
171 <https://bitbucket.org/feeldead/gfold/>) and the GENCODE annotation file of the human genome  
172 ([gencode.v19.annotation.gtf](https://www.gencodegenes.org/); <https://www.gencodegenes.org/>) (Feng *et al.*, 2012; Dobin *et al.*, 2013). The differential  
173 expression of genes was then calculated with GFOLD-diff bioinformatics pipeline. For this final step, GFOLD pipeline  
174 values were the mean of three independent samples The heatmap representation was carried out using the Xlstat software  
175 (<https://www.xlstat.com/fr/solutions/biomed>)

### 176 **Flow cytometry**

177 The quantity of H<sub>2</sub>O<sub>2</sub> was estimated using an indicator of ROS in cells (CM-H<sub>2</sub>DCFDA; reference #C6827), and RNS  
178 derivatives using a nitric oxide indicator (DAF-FM; reference #D23841) according to the manufacturer's instructions  
179 (Thermo Fisher Scientific). Whole-cell fluorescence intensity was quantified by flow cytometry using a BD FACSCalibur  
180 (BD Biosciences, Grenoble, France) with 10,000 events recorded. The final data were analyzed using the FlowLogic  
181 Software (Miltenyi Biotec GmbH, Bergisch Gladbach, Germany). Each condition was duplicated, and at least three  
182 independent experiments were carried out.

183

### 184 **H2A.X phosphorylation on Serine 139**

185 Differentiated HepaRG cells were treated with nitropyrazole-derived HEDMs. After trypsinization, cells were resuspended  
186 in 500 µL of 1X Assay Buffer (included in the kit, Catalog No. MCH200101) per one million cells. Equal parts of Fixation  
187 Buffer were added to cell suspensions. Cells were then permeabilized by adding 1 mL ice-cold 1X Permeabilization Buffer  
188 per one million cells and incubated on ice for 5 min. After washing, cells were resuspended in 90 µL of 1X Assay Buffer.  
189 10 µL of the antibody working cocktail solution (5 µL of antiphospho-histone H2A.X (Ser139), Alexa Fluor® 555 and 5  
190 µL of anti-histone H2A.X, PECy5 conjugated) were added to each experimental condition and incubated for 30 min at  
191 room temperature (RT) in the dark. After washing, the fluorescence of nuclear foci was visualized via the Muse™ Cell  
192 Analyzer using the onscreen instructions.

193

### 194 **Quantification of LDH, glucose, and lactate**

195 Using the ARCHITECT C16000 Clinical Chemistry Analyzer (Abbott Laboratories, Chicago, Illinois, US), and their  
196 validated CE-IVD kits, lactate dehydrogenase (LDH), glucose (GLU) and lactate contents were quantified (Guyot *et al.*,  
197 2018). Each condition was duplicated, and at least three independent experiments were carried out. Glucose consumption  
198 is defined as the difference between the initial glucose concentration and the glucose remaining at the end of the experiment.  
199 Similarly, the secretion of lactate and LDH are calculated by the difference between their initial and final concentrations.



200

201 **Cell cycle exploration**

202 HepaRG cells in a proliferative phase were treated with Nitropyrazole-derived HEDMs for 24 h. We then added 30  $\mu$ M of  
203 5-bromo-2'-deoxyuridine (BrdU) for 1 h. After trypsinization, cells were washed with PBS 1X, and fixed using 70%  
204 ethanol. Again, cells were washed with PBS 1X and treated with 2 mol/L HCl for 20 min at RT. Cells were washed with  
205 0.5% BSA 0.5% Tween in PBS (PBT), incubated with an anti-BrdU conjugated with FITC (BD Biosciences; dilution 1/10  
206 in PBT) for 30 min at RT in the dark, and then washed with PBT. After resuspension of cells into 100  $\mu$ L of PBS, cells  
207 were incubated for 30 min in the dark at RT with RNase at a final concentration of 100  $\mu$ g/mL (Sigma-Aldrich St. Louis,  
208 MO US). 300  $\mu$ L of PBS were then added and the cells were incubated with 20  $\mu$ g/mL propidium iodide (PI). Whole-cell  
209 fluorescence intensity was measured by FACS using a BD LSR Fortessa™ flow cytometer (BD Biosciences, Grenoble,  
210 France) with 10,000 events recorded. The final data were analyzed using the FlowLogic Software (Miltenyi Biotec GmbH,  
211 Bergisch Gladbach, Germany). Each condition was replicated, and at least three independent experiments were carried out.

212

213 **Apoptosis assay (Annexin V labeling)**

214 Differentiated HepaRG cells were treated with Nitropyrazole-derived HEDMs for 24 h and 72 h. Cells were trypsinized  
215 and diluted to 100,000 cells/mL in a buffer (PBS 1x + SVF 1%). 100  $\mu$ L of the Muse™ Annexin V & Dead Cell Reagent  
216 Kit; MCH100105) was added to 100  $\mu$ L of each condition. Following 20 min of staining at RT, data were acquired by flow  
217 cytometry with the Muse™ Cell Analyzer using the onscreen instructions.

218

219 **Targeted metabolomics**

220 At the end of the exposition of differentiated HepaRG cells, the culture medium was removed and cells were washed three  
221 times with cold PBS 1X. For samples destined to nucleotide determination, cold methanol/water (v/v: 70/30) was added,  
222 while in samples used for the determination of other metabolites, cold methanol/water (v/v: 70/30) and 3% formic acid  
223 were added. Samples were stored at -80°C until analysis. Sample preparation was performed as follows: labeled internal  
224 standards (4 for nucleotides and 27 for other metabolites) were added to cellular extracts which were vigorously vortexed  
225 and centrifuged for 10 min at 13,000 g. Supernatants were evaporated to dryness under nitrogen at 37 °C. The residues  
226 were resuspended in 200  $\mu$ L and 100  $\mu$ L of mobile phase before injection, for metabolites and nucleotides, respectively.  
227 Targeted metabolomic analyzes were performed by liquid chromatography coupled with a tandem high resolution mass  
228 spectrometer (Q-Exactive Plus Orbitrap, Thermo Scientific, Bremen, Germany). The high resolution mass spectrometer  
229 was operated alternatively in positive and negative ionization mode. Full scan and dd-MS<sup>2</sup> (data dependent MS/MS) modes

230 were used with a resolution set at 70,000 and 17,500, respectively. Metabolites were identified using retention time,  
231 accurate mass of parent compound, isotopic pattern and daughter ions.

232

### 233 **Statistics**

234 All statistical analyses were performed using the GraphPad InStat software 7.00 (GraphPad Software; La Jolla, CA USA).  
235 The non-parametric test for significance was performed when the number of samples (N) was below 30. Non-parametric  
236 tests for non-normalized data or for  $n < 30$  and a two-way ANOVA were performed for normalized data. A 2-sided P-value  
237 of  $< 0.05$  was considered statistically significant.

## 238 **RESULTS**

239

### 240 **Effect of nitropyrazole-related molecules on proliferation and viability of rodent and human cell models**

241 HEDM-induced cytotoxicity, measured either *via* MTT assays or using the xCELLigence system for the nitropyrazole-  
242 derived HEDMs listed in Table 1, was determined in murine L5178Y TK +/- clone (3.7.2C) and BALB/3T3 clone A31  
243 cells and in Chinese hamster CHO-K1 cells (Table 2; Supplementary Figure S1a-c), as well as in human PFS04062  
244 fibroblasts (Table 2; Supplementary Figure S1d) and human hepatocytes-like HepaRG cells (Table 3; Supplementary  
245 Figure S1e-f). Unfortunately, L5178Y TK +/- clone (3.7.2C) BALB/3T3 clone A31 cells could not be tested using the  
246 xCELLigence analysis since they did not adhere to the chamber, while the CRC05 human fibroblasts were not tested. For  
247 some xCELLigence experiments, the highest dose of the HEDMs was tested or the determined MTT CI50 concentration.  
248 The xCELLigence allowed us to confirm the MTT findings. However, data (presented in Table 2) revealed that, except for  
249 1-nitropyrazole (1-NP), both techniques led to very similar results. Indeed, the half maximum inhibitory concentration or  
250  $IC_{50}$  of the nitropyrazole-derived HEDMs obtained *via* the MTT assay when applied to the xCELLigence system blocked  
251 cell proliferation in a dose-dependent manner and in the same range as the MTT assay, except for 1-NP which appeared to  
252 have no effect on cells in the latter test. This could be due to the different parameters measured (mitochondrial activity for  
253 the MTT assay *vs* cellular confluence for the xCELLigence) or to the assay conditions (different surfaces of adhesion...).

254 The first noteworthy result is the clear cytotoxic effect of 1,3-dinitropyrazole (1,3-DNP) and 3,4,5-trinitropyrazole (3,4,5-  
255 TNP) on all three rodent cell models compared to the other four nitropyrazole-derived HEDMs. This is illustrated by the  
256 clear shift in cell viability curves (Supplementary Figure S1a-c) after the incubation of cells with 1,3-DNP and 3,4,5-TNP  
257 concentrations 50-200 fold lower (0.002-0.04 mM) than 1-NP, 3-NP, 3,5-DNP, 4-NP and 1-methyl 4-nitropyrazole (1-  
258 Met-4-NP) (0.4- > 10 mM; Table 2). Though the effects of 3,5-DNP and 1-Met-4-NP were difficult to differentiate between  
259 these cell lines, (i) BALB/3T3 clone A31 cells were more resistant to 1-NP, 3-NP and 4-NP than L5178Y TK +/- clone

260 (3.7.2C) and CHO-K1 cells, and (ii) 1-NP affected L5178Y TK +/- clone (3.7.2C) cells more than CHO-K1 cells, while  
261 this was the opposite for 3-NP and was indistinctive for 4-NP (Table 2). The cytotoxic effects of HEDM molecules were  
262 independently confirmed in CHO-K1 using the xCELLigence assay.

263 In human adult PFS04062 and CRC05 fibroblasts, the IC<sub>50</sub> were in the same range for 3-NP, 3,5-DNP, 4-NP and 1-Met-  
264 4-NP (except in CRC05 in which the level of cytotoxicity was not be determined). Overall, a 10-fold greater IC<sub>50</sub> was  
265 measured in human fibroblasts than in animal fibroblasts, suggesting a stronger resistance of human dermic fibroblasts to  
266 the nitroprazole-derived HEDMs. Furthermore, in the case of PFS04062 the effect of these molecules was more marked  
267 when looking at the proliferating cell index (CI) of the xCELLigence method (Table 2). Once again, the most cytotoxic  
268 molecule was 1,3-DNP, followed by 3,4,5-TNP (as evidenced in the Supplementary Figure S1d). This was also true for  
269 human HepaRG hepatocytes, both in a proliferative and differentiated stage (Table 3; Supplementary Figure S1e-f).  
270 However, these two stages displayed several interesting differences as 1,3-DNP and 1-NP had a 10-fold and 3,5-NP had  
271 an ~4-fold greater effect on proliferative cells, while 3,4,5-TNP had a similar IC<sub>50</sub> in both stages (Table 3).

272 Finally, the impact of Nitroprazole-derived HEDMs on the cell cycle of proliferative HepaRG cells was studied for 24 h,  
273 and a cytostatic effect of 1,3-DNP, 3,4,5-TNP and 3,5-DNP was found. These molecules blocked the cell cycle of HepaRG  
274 cells in the S and G2M phases, and decreased the proportion of HepaRG cells in the G1 phase. In contrast, exposure to 1-  
275 NP led to a decrease in cells in the S phase, indicating an impairment in DNA replication. The other molecules did not  
276 modify the proportion of cells in the different phases (Table 3). Altogether, our findings led us to propose the resulting  
277 cytotoxicity ranking in all of the cell lines tested above: 1,3-DNP>>> 3,4,5-TNP>> 3,5-DNP ≅ 1-NP >3-NP = 4-NP = 1-  
278 Met-4-NP.

279

### 280 **Effects of Nitroprazole-derived HEDMs on physiological pathways in differentiated HepaRG cells**

281 Owing to the vital role played by hepatocytes in the biotransformation of xenobiotics and to the frequent accumulation of  
282 toxic molecules/derivatives in these cells, the remainder of our study focuses on the physiopathological effects of  
283 Nitroprazole-derived HEDMs on differentiated HepaRG cells. Consistently, we attempted to mimic a sub-chronic  
284 exposure to non-deadly concentrations of these HEDMs and verified their impact on cellular functions (major cell signaling  
285 pathways).

286 We initially evaluated the effect doses of nitroprazole-derivatives over 24 h on the rate of cell death, by measuring LDH  
287 release into the medium of differentiated HepaRG cells. Indeed, LDH release is a validated early biomarker for the  
288 induction of cytolysis and can be measured via flow cytometry. Under our experimental conditions no detectable cytolysis  
289 was observed in differentiated Hepa-RG cells (Supplementary Table S1). Under these conditions, we studied the biological

290 effect of the highest doses of HEDMs could experimentally be used. To confirm that this was not due to a lack of uptake  
291 of the nitroprazole-derived HEDMs, the intracellular accumulation of Nitroprazole-derived HEDMs was carried out by  
292 liquid chromatography coupled with tandem high resolution mass spectrometry (LC-HRMS). Four nitroprazole-derived  
293 HEDMs were quantified, clearly showing an uptake of these compounds into cells (Supplementary Table S2).  
294 Unfortunately, we were unable to quantify 1-NP, 1,3-DNP and 1-Met-4-NP using LC-HRMS, since they do not contain  
295 any ionizable groups (Bader *et al.*, 1998; Coombs and Schillack, 1998). However, since the other nitroprazole-derived  
296 HEDMs were taken up (Supplementary Table S2), this strongly suggests that these compounds should also penetrate into  
297 cells and reassured us as to our interpretations of our regulatory findings even if no biological effects were observed.

298 As shown above, 1,3-DNP, 3,4,5-TNP and 3,5-DNP blocked the cell cycle at the S and G2M stages in proliferative cells.  
299 Though differentiated HepaRG cells reached confluence after 24 h incubation with the three nitroprazole-derived  
300 HEDMs, these were able to modify the level of expression of transcripts of genes involved in cell cycle regulation  
301 (Supplementary Figure S2). The strongest transcript up-regulations (represented in red on the heat-map in Supplementary  
302 Figure 2S) were observed with 1,3-DNP.

303 In parallel, the expression levels of genes involved in death pathways (necrosis, senescence, autophagy and apoptosis) were  
304 analyzed and little modifications in autophagy, necrosis and senescence were observed (Table 4). When examining the  
305 apoptosis signaling pathway, we subdivided the actors according to their pro- and anti-apoptotic functions (Supplementary  
306 Figure S3), and found some variations at the transcriptomic level both for pro- and anti-apoptotic factors (Supplementary  
307 Figure S3). Based on Annexin V labeling (see Materials and Methods for details) we studied the number of cells undergoing  
308 early and late stage apoptosis after 24 h and 72 h incubation with nitroprazole-derived HEDMs but found no differences  
309 with controls (vehicles) under our experimental conditions (Table 5), suggesting that the variations in gene expression  
310 levels were not sufficient to increase cell death rates.

311

### 312 **Identification of the initial events leading to modifications in physiological processes**

313 In parallel, we also evaluated the impact of these HEDMs on physiopathological pathways including known genotoxic  
314 pathways responsible for cancer initiation (first step in the carcinogenesis process), oxidative stresses due to reactive  
315 nitrogen species (RNS) and reactive oxygen species (ROS) production since they are largely involved in toxicological  
316 pathways. We also studied metabolite biosynthesis, such as the amino acids, nucleic acid derivatives and organic acid  
317 derivatives, since they modify the proliferation rate and energy cellular biosynthesis. The genotoxicity of nitroprazole-  
318 derived HEDMs was indirectly studied in human differentiated HepaRG cells based on two complementary approaches,  
319 namely by assessing (i) the regulation of genes involved in DNA repair pathways and (ii) the number of nuclear foci upon

320 phosphorylation of the Serine P139 residue on the H2AX protein (a marker of activation of the double-strand break DNA  
321 repair system) using the Muse™ H2A.X. Clearly, an up-regulation in the expression levels of DNA repair genes was  
322 observed after 24 h exposure to non-deadly concentrations of 1,3-DNP, 3,4,5-TNP and 3,5-DNP, while only a slight down  
323 regulation was noted for the other molecules (Fig. 1a). Furthermore, though no increase in the number of  $\gamma$ -H2AX foci was  
324 quantified after 2 h exposure to nitropyrazole-derived HEDMs, at 24 h an increase was observed for 3-NP, 1,3-DNP, 3,4,5-  
325 TNP and 3,5-DNP (Fig. 1b). This effect was stronger for 3,4,5-TNP.

326 To study the putative drivers of genotoxicity, both ROS ( $H_2O_2$ ) and RNS derivatives were measured in differentiated  
327 HepaRG cells exposed to nitropyrazole-derived HEDMs. The expression levels of genes implicated in oxidative and radical  
328 pathways were inversely regulated by the cytotoxic nitropyrazole-derived HEDMs and the weakly cytotoxic molecules  
329 (Fig. 2a). We observed an increase in expression levels of genes encoding proteins involved in the protection against  
330 oxidative stresses, including GSTA1 and SOD, after incubation with 1-NP, 3-NP, 4-NP, 1-Met-4-NP, while these  
331 transcripts were down-regulated by the cytotoxic nitropyrazole-derived HEDMs(1,3-NP, 3,4,5-TNP and 3,5-DNP). These  
332 findings indicate that oxidative stress pathways may be involved in the cellular cytotoxicity caused by these nitropyrazole-  
333 derived HEDMs (Fig. 2a). ROS production was then quantified after 90 min using CM- $H_2$ DCFDA probes (Fig. 2b), the 1  
334 mM was the highest tested concentration of HEDMs, we could test under our experimental condition (we limited the  
335 percentage of DMSO exposure to 0.5%). Both 1,3-DNP and 3,4,5-TNP significantly increased cellular ROS levels, while  
336 the other nitropyrazole-derived HEDMs displayed no significant modifications under our experimental conditions. Using  
337 DAF-FM probes, intracellular RNS levels were also quantified after 60 min following the same assay conditions as for  
338 ROS measurement. Interestingly, 1,3-DNP, 3,4,5-TNP and 3,5-DNP were able to significantly increase RNS production  
339 in cells, while 1-NP, 4-NP, and 1-Met-4-NP did not induce any change for RNS production at 1 mM and 3NP induced a  
340 decrease for RNS production at a final assay concentration of 1 mM (Fig. 2c).

341

### 342 **Metabolomic findings**

343 Having observed an increase in ROS production in differentiated HepaRG cells treated with 1,3-DNP and 3,4,5-TNP, as  
344 well as an increase in RNS production, we assumed that these molecules may modify the production of energy by cells  
345 (ATP, amino acids, acid organic). Lactate secretion and glucose consumption by differentiated HepaRG cells exposed to  
346 varying concentrations of nitropyrazole-derived HEDMs were quantified after 6 h, 24 h and 48 h. A significant increase in  
347 lactate secretion into the medium was only observed for 1-NP, 4-NP, 3,5-DNP and 3-NP after 24 h and 48 h, while glucose  
348 levels strongly decreased after 48 h exposure (Supplementary Table S3). Additionally, some transcripts of genes involved  
349 in energy producing pathways were up-regulated following exposure to 3-NP, 1-NP and 1-Met-4-NP nitropyrazole-derived

350 HEDMs, whereas the other nitropyrazole-derived HEDMs slightly down-regulated these metabolic pathway actors (Fig.  
351 3a). To complete this transcriptomic study, pools of approximately 40 endogenous physiological compounds were  
352 measured (expressed in fold-change) after 36 h of exposure to these nitropyrazole molecules. At this time it was also  
353 performed the transcriptional and post-transcriptional effects of the HEDMs on metabolomics functions of the cells. Very  
354 few modifications in endogenous pools were observed (Supplementary Table S4). Creatine, cysteine, N-acetylspermidine  
355 pools were increased under 1,3-DNP and 3,5-DNP treatments. Alanine pool was increased under 3,5-DNP and 3-NP  
356 treatments. 3,4,5-TNP treatment decreased 5-hydroxyindolacetic acid and putrescine pools (Supplementary Table S4 and  
357 Fig. 3b).

358

## 359 **DISCUSSION**

360 To validate the use of novel, more powerful and stable HEDMs in military or civilian applications, their toxic side effects  
361 have to be tested following rigorous OECD guidelines. Here, we initially tested the cytotoxicity of seven nitropyrazole-  
362 derived molecules; 1-nitropyrazole (1-NP), 3-nitropyrazole (3-NP), 1,3-dinitropyrazole (1,3-DNP), 3,5-dinitropyrazole  
363 (3,5-DNP), 3,4,5-trinitropyrazole (3,4,5-TNP), 4-nitropyrazole (4-NP), and 1-methyl 4-nitropyrazole (1-Met-4-NP), using  
364 three animal cell lines listed in the database of the European Centre for the Validation of Alternative Methods (ECVAM)  
365 and OCDE organization (OECD - Guidance Document on Good In Vitro Method Practices (GIVIMP)). These databases  
366 enable researchers to perform alternative *in vitro* toxicity tests on previously validated models, thus improving their  
367 acceptance by regulators and facilitating the toxicological assessment/comparison of molecules. Based on their IC<sub>50</sub>, we  
368 determined the cytotoxic ranking for all of the nitropyrazole-derived HEDMs in the three rodent cell lines (BALB/3T3  
369 clone A31, CHO-K1 and L5178Y TK +/- clone (3.7.2C)), exposing 1,3-DNP and 3,4,5-TNP as the most cytotoxic.  
370 Interestingly, this ranking was identical for these cell lines, as well as for human fibroblasts (CRC05, PFS04062) and  
371 hepatocytes (HepaRG). HepaRG cells were then more extensively studied, as they strongly express biotransformation  
372 enzymes (Aninat *et al.*, 2006; Antherieu *et al.*, 2012) and are most likely to accumulate xenobiotics (Le Vee *et al.*, 2013).  
373 The cytotoxicity ranking for these cells resembled that observed with other cell lines with 1,3-DNP, 3,5-DNP and 3,4,5-  
374 TNP having the strongest effects. To ascertain whether this effect was due to an increase in cell death or to a cytostatic  
375 effect, we studied their impact on the cell cycle and clearly showed that 1,3-DNP, 3,5-DNP and 3,4,5-TNP blocked cells  
376 in the S and G2M stage, while the proportion of cells in S phase strongly decreased with 1-NP. This clearly indicated that  
377 these molecules block the proliferation pathway. Interestingly, after differentiation their level of cytotoxicity largely  
378 decreased suggesting that the biotransformation capacities of HepaRG cells metabolized and eliminated these molecules.

379 Differentiated HepaRG cells is currently used and validated by the ECVAM to explore the hepatotoxic effects of drugs  
380 (Aninat et al. 2006; Anthérieu et al. 2011, 2012; Sharanek et al. 2014; Truisi et al. 2015; Pomponio et al. 2015). The  
381 biotransformation capability of differentiated HepaRG cells had a particular interest here since previous works on  
382 nitrofurantoin or nitroimidazole indicated that nitro-group determines hepatic cytotoxicity through reactive intermediates  
383 such as nitroso and hydroxylamine derivatives (Li *et al.*, 2019; Nepali *et al.*, 2019). Moreover, TNT is a known genotoxic  
384 (Ahlborg et al. 1988), we were initially interested in investigating the genotoxicity of the nitropyrazole-derived HEDMs,  
385 and this is usually *via* the Ames and the micronuclei tests. The former is based on bacterial cells, and the latter principally  
386 murine cell lines. The genotoxicity of some nitro imidazole derivatives, such as benznidazole (2-nitro-N-(phenylmethyl)-  
387 1H-imidazole-1-acetamide), have already been described in the Ames test (Ferreira and Ferreira, 1986). This genotoxicity  
388 effect has been directly linked to nitroreductases expressed in salmonella. Interestingly, it has been argued that the lower  
389 capacity of mammalian cells to perform nitroreduction decreases the genotoxic risk of 5-nitromegazol (Buschini *et al.*,  
390 2007). Then, we proposed to evaluate genotoxicity effects using mammalian cells. Owing to the difference in cytotoxicity  
391 between species found in our first experiments, we evaluated this parameter in the human differentiated HepaRG model  
392 by (i) quantifying the phosphorylation of Ser139 on H2A.X, a hallmark of DNA repair machinery activation, and (ii)  
393 through transcriptomic analysis to highlight DNA repair pathway genes regulated by these HEDMs. Both techniques  
394 revealed that 1,3-DNP and 3,4,5-TNP activated DNA reparation mechanisms. This effect was attended as 5-nitroimidazol  
395 compounds increase DNA damages through the so-called futile cycle, i.e. one electron reduction of the drug leads to the  
396 production of nitro radical anions which in the presence of oxygen are oxidized and may generate reactive oxygen species  
397 (ROS) (Re *et al.*, 1997; Nepali *et al.*, 2019). The nitro radical anion and nitroso derivatives, or esterified hydroxylamine  
398 (e.g., sulfate derivatives) are associated with the mutagenicity (Bolt *et al.*, 2006). Superoxide anions, hydrogen peroxide,  
399 and hydroxyl radicals formed during the redox cycling of the nitro radical anion may also lead to carcinogenicity (Nepali  
400 *et al.*, 2019). Then, to identify in our present study the early driver of this genotoxicity, we quantified the production of  
401 radical stresses (RNS and ROS) in HepaRG cells and concomitantly evaluated the expression of genes involved in these  
402 pathways. Our findings strongly suggest the role of radical stress in nitropyrazole-derived genotoxicity, corroborating  
403 previous studies on TNT but also on 5-nitroimidazole (Bolt *et al.*, 2006; Nepali *et al.*, 2019). This hypothesis was supported  
404 by several reports in which the generation of oxidative stress by diazinon, was decreased by antioxidant molecules co-  
405 exposition in various cellular models (Ahmadi *et al.*, 2015; Ahmadi and Shadboorestan, 2016; Karamian *et al.*, 2016).  
406 Since oxidative stress plays a crucial role in the pathophysiology of tumors, in our work support, the use of appropriated  
407 measures for the prevention of occupational hazards of 1,3-DNP and 3,4,5-TNP compounds. Since the other HEDMs

408 molecules contain nitro radical anion, actions under the precautionary principle should be implemented (Nepali *et al.*,  
409 2019)

410 Similarly, to TNT studies, we explore the molecular toxicological mechanisms of the HEDMs. Indeed, one of the possible  
411 mechanisms of toxicity of TNT and some of its metabolic intermediates is the generation of reactive oxygen species that  
412 cause injury to the lens leading to the formation of cataracts and lipid peroxidation in the live. This is supported by the fact  
413 that at high levels in the air, workers involved in the production of TNT experience anemia and liver function abnormalities,  
414 as well skin irritation and cataracts after long-term exposure (Letzel *et al.*, 2003). Since, industries have been strongly  
415 recommended to limit the use of *in vivo* models, it is of vital importance that *in vitro* strategies are developed and that data  
416 can be transposed to *in vivo* situations, such as through the use of transcriptomics (Deng *et al.*, 2010). Indeed, these authors  
417 revealed that gene regulatory networks obtained from an *in vitro* system could predict *in vivo* functions and mechanisms.  
418 In their study, 341 common transcripts were differentially expressed *in vitro* and *in vivo* in response to TNT, and they  
419 reported that inhibiting PTTG1 and its targeted cell cycle-related genes in the liver could be a key mechanism for TNT-  
420 induced liver toxicity. These authors also proposed that the development of mathematical simulation tools could improve  
421 *in vitro* data interpretation (Deng *et al.*, 2010). In the present study, we also clearly established the regulation of genes  
422 modulating common pathways *in vitro*, and provided a complete overview of the principal toxic effects and physiological  
423 impacts of nitropyrazole-derived HEDMs in HepaRG cells. Furthermore, most of the changes in gene expression observed  
424 after nitropyrazole exposure were accompanied by modifications in functional biomarkers, including RNS and ROS pools,  
425 H2A.X serine 139 phosphorylation, and activation of apoptosis. This approach thus seems to be of great interest, and merits  
426 further investigation.

427 In agreement with our transcriptomic approach, researchers have utilized a novel high-throughput transcriptomics (HTT)  
428 platform to apply the interpretive power of concentration-response modeling with exposures to reference compounds in  
429 both differentiated and non-differentiated human HepaRG cell cultures. They explored transcriptomic characteristics  
430 distinguishing liver injury compounds, and assess impacts of differentiation state of HepaRG cells on baseline and  
431 compound-induced responses (e.g., metabolically-activated), and identify and resolve reference biological-response  
432 pathways through benchmark concentration modeling. Similarly to our data, impacts of cellular differentiation state  
433 (proliferated vs. differentiated) were revealed on baseline drug metabolizing enzyme expression, hepatic receptor signaling,  
434 and responsiveness to metabolically-activated toxicants (e.g., cyclophosphamide, benzo(a)pyrene, and aflatoxin B1)  
435 (Ramaiahgari *et al.*, 2019). Taken together, these findings confirmed the predictive value of toxicological level obtained  
436 using *in vitro* liver models avoiding the use of *in vivo* experiments.



437 Since non-alcoholic Fatty Liver Disease (NAFLD) is a frequently encountered Drug-Induced Liver Injury (DILI). Although  
438 this stage of the disease is reversible, it can lead to irreversible damage provoked by non-alcoholic steatohepatitis (NASH),  
439 fibrosis and cirrhosis. Therefore, the assessment of NAFLD is a paramount objective in toxicological screenings of new  
440 industrial compounds. Recently, it has been reported a metabolomic fingerprint of NAFLD induced in HepaRG cells at  
441 four dosing schemes by a reference toxicant, sodium valproate (NaVPA), using liquid-liquid extraction followed by liquid  
442 chromatography and accurate mass-mass spectrometry (LC-AM/MS). Increased levels of S-adenosylmethionine and  
443 mono-acetylspermidine in combination with only a moderate increase in triglycerides was observed first and in second  
444 time, spermidines, creatine, and acetylcholine were modified, signing a steatotic progression. In our report, only creatine,  
445 cysteine, N-acetylspermidine pools were increased under 1,3-DNP and 3,5-DNP treatments were modified, suggesting a  
446 possible risk of steatosis activation (Cuykx *et al.*, 2018).

447 In conclusion, the present study demonstrated the cytotoxicity of seven nitropyrazole-derived HEDMs in differentiated  
448 HepaRG cells and particularly the genotoxic effect of 1,3-DNP and 3,4,5-TNP that increase DNA double-strand breaks,  
449 likely *via* the production of ROS/RNS molecules. This study shows that the position of nitro-group on the pyrazole nucleus  
450 have an influence on the cytotoxicity level as previously demonstrated for nitro-imidazole derivatives (Boechat *et al.*,  
451 2015).

452

453 **Compliance with ethical standards**

454 Not applicable

455

456 **Conflict of interest**

457 Authors declare no conflict of interest

458

459 **Funding**

460 This work was supported by institutional grants from ArianeGroup. LG was recipient of fellowships from ArianeGroup.

461

## References

- 462  
463 Ahmadi, A., Shadboorestan, A., 2016. Oxidative stress and cancer; the role of hesperidin, a citrus  
464 natural bioflavonoid, as a cancer chemoprotective agent. *Nutr Cancer* **68**, 29-39.
- 465 Ahmadi, A., Shadboorestan, A., Nabavi, S.F., Setzer, W.N., Nabavi, S.M., 2015. The Role of  
466 Hesperidin in Cell Signal Transduction Pathway for the Prevention or Treatment of Cancer.  
467 *Curr Med Chem* **22**, 3462-3471.
- 468 Aninat, C., Piton, A., Glaise, D., Le Charpentier, T., Langouet, S., Morel, F., Guguen-Guillouzo, C.,  
469 Guillouzo, A., 2006. Expression of cytochromes P450, conjugating enzymes and nuclear  
470 receptors in human hepatoma HepaRG cells. *Drug Metab Dispos* **34**, 75-83.
- 471 Antherieu, S., Chesne, C., Li, R., Guguen-Guillouzo, C., Guillouzo, A., 2012. Optimization of the  
472 HepaRG cell model for drug metabolism and toxicity studies. *Toxicol In Vitro* **26**, 1278-1285.
- 473 Bader, M., Goen, T., Muller, J., Angerer, J., 1998. Analysis of nitroaromatic compounds in urine by  
474 gas chromatography-mass spectrometry for the biological monitoring of explosives. *J*  
475 *Chromatogr B Biomed Sci Appl* **710**, 91-99.
- 476 Bell, C.C., Lauschke, V.M., Vorrink, S.U., Palmgren, H., Duffin, R., Andersson, T.B., Ingelman-  
477 Sundberg, M., 2017. Transcriptional, Functional, and Mechanistic Comparisons of Stem Cell-  
478 Derived Hepatocytes, HepaRG Cells, and Three-Dimensional Human Hepatocyte Spheroids  
479 as Predictive In Vitro Systems for Drug-Induced Liver Injury. *Drug Metab Dispos* **45**, 419-  
480 429.
- 481 Boechat, N., Carvalho, A.S., Salomao, K., Castro, S.L., Araujo-Lima, C.F., Mello, F.V., Felzenszwalb,  
482 I., Aiub, C.A., Conde, T.R., Zamith, H.P., Skupin, R., Haufe, G., 2015. Studies of genotoxicity  
483 and mutagenicity of nitroimidazoles: demystifying this critical relationship with the nitro  
484 group. *Mem Inst Oswaldo Cruz* **110**, 492-499.
- 485 Bolt, H.M., Degen, G.H., Dorn, S.B., Plottner, S., Harth, V., 2006. Genotoxicity and potential  
486 carcinogenicity of 2,4,6-TNT trinitrotoluene: structural and toxicological considerations. *Rev*  
487 *Environ Health* **21**, 217-228.
- 488 Buschini, A., Giordani, F., de Albuquerque, C.N., Pellacani, C., Pelosi, G., Rossi, C., Zucchi, T.M.,  
489 Poli, P., 2007. Trypanocidal nitroimidazole derivatives: relationships among chemical  
490 structure and genotoxic activity. *Biochem Pharmacol* **73**, 1537-1547.
- 491 Chatterjee, S., Deb, U., Datta, S., Walther, C., Gupta, D.K., 2017. Common explosives (TNT, RDX,  
492 HMX) and their fate in the environment: Emphasizing bioremediation. *Chemosphere* **184**, 438-  
493 451.
- 494 Coombs, M., Schillack, V., 1998. Determination of trinitrotoluene and metabolites in urine by means  
495 of gas-chromatography with mass detection. *Int Arch Occup Environ Health* **71 Suppl**, S22-  
496 25.
- 497 Cuykx, M., Claes, L., Rodrigues, R.M., Vanhaecke, T., Covaci, A., 2018. Metabolomics profiling of  
498 steatosis progression in HepaRG((R)) cells using sodium valproate. *Toxicol Lett* **286**, 22-30.
- 499 Dalinger, I.L., Vatsadze, I.A., Shkineva, T.K., 2010. The specific reactivity of 3,4,5-trinitro-1H-  
500 pyrazole. *Mendeleev Commun.* **20**, 253-254.
- 501 Deng, Y., Ai, J., Guan, X., Wang, Z., Yan, B., Zhang, D., Liu, C., Wilbanks, M.S., Escalon, B.L.,  
502 Meyers, S.A., Yang, M.Q., Perkins, E.J., 2014. MicroRNA and messenger RNA profiling  
503 reveals new biomarkers and mechanisms for RDX induced neurotoxicity. *BMC Genomics* **15**  
504 **Suppl 11**, S1.
- 505 Deng, Y., Johnson, D.R., Guan, X., Ang, C.Y., Ai, J., Perkins, E.J., 2010. In vitro gene regulatory  
506 networks predict in vivo function of liver. *BMC Syst Biol* **4**, 153.
- 507 Dobin, A., Davis, C.A., Schlesinger, F., Drenkow, J., Zaleski, C., Jha, S., Batut, P., Chaisson, M.,  
508 Gingeras, T.R., 2013. STAR: ultrafast universal RNA-seq aligner. *Bioinformatics* **29**, 15-21.
- 509 Feng, J., Meyer, C.A., Wang, Q., Liu, J.S., Shirley Liu, X., Zhang, Y., 2012. GFOLD: a generalized  
510 fold change for ranking differentially expressed genes from RNA-seq data. *Bioinformatics* **28**,  
511 2782-2788.

512 Ferreira, R.C., Ferreira, L.C., 1986. Mutagenicity of CL 64855, a potent anti-Trypanosoma cruzi drug.  
513 Mutat Res **171**, 11-15.

514 Gust, K.A., Lotufo, G.R., Stanley, J.K., Wilbanks, M.S., Chappell, P., Barker, N.D., 2018.  
515 Transcriptomics provides mechanistic indicators of mixture toxicology for IMX-101 and IMX-  
516 104 formulations in fathead minnows (*Pimephales promelas*). Aquat Toxicol **199**, 138-151.

517 Guyot, L., Honorat, M., Jacob, G., Bardel, C., Tod, M., Puisieux, A., Guitton, J., Payen, L., 2018.  
518 Toxicokinetics and tolerance of a high energy material 3,4,5-trinitroproazole (TNP) in mice.  
519 Toxicol Appl Pharmacol **355**, 103-111.

520 Karamian, A., Shokrzadeh, M., Ahmadi, A., 2016. The potential chemoprotective effects of melatonin  
521 against genotoxicity induced by diazinon in human peripheral blood lymphocytes. Toxicol Ind  
522 Health **32**, 360-366.

523 Le Vee, M., Noel, G., Jouan, E., Stieger, B., Fardel, O., 2013. Polarized expression of drug transporters  
524 in differentiated human hepatoma HepaRG cells. Toxicol In Vitro **27**, 1979-1986.

525 Letzel, S., Goen, T., Bader, M., Angerer, J., Kraus, T., 2003. Exposure to nitroaromatic explosives and  
526 health effects during disposal of military waste. Occup Environ Med **60**, 483-488.

527 Li, H., Zhang, Z., Yang, X., Mao, X., Wang, Y., Wang, J., Peng, Y., Zheng, J., 2019. Electron  
528 Deficiency of Nitro Group Determines Hepatic Cytotoxicity of Nitrofurantoin. Chem Res  
529 Toxicol **32**, 681-690.

530 Limonciel, A., Ates, G., Carta, G., Wilmes, A., Watzele, M., Shepard, P.J., VanSteenhouse, H.C.,  
531 Seligmann, B., Yeakley, J.M., van de Water, B., Vinken, M., Jennings, P., 2018. Comparison  
532 of base-line and chemical-induced transcriptomic responses in HepaRG and RPTEC/TERT1  
533 cells using TempO-Seq. Arch Toxicol **92**, 2517-2531.

534 Lotufo, G.R., Stanley, J.K., Chappell, P., Melby, N.L., Wilbanks, M.S., Gust, K.A., 2018. Subchronic,  
535 chronic, lethal and sublethal toxicity of insensitive munitions mixture formulations relative to  
536 individual constituents in *Hyalella azteca*. Chemosphere **210**, 795-804.

537 Mesnage, R., Biserni, M., Balu, S., Frainay, C., Poupin, N., Jourdan, F., Wozniak, E., Xenakis, T.,  
538 Mein, C.A., Antoniou, M.N., 2018. Integrated transcriptomics and metabolomics reveal  
539 signatures of lipid metabolism dysregulation in HepaRG liver cells exposed to PCB 126. Arch  
540 Toxicol **92**, 2533-2547.

541 Moedas, M.F., Adam, A.A.A., Farelo, M.A., L, I.J., Chamuleau, R., Hoekstra, R., Wanders, R.J.A.,  
542 Silva, M.F.B., 2017. Advances in methods for characterization of hepatic urea cycle enzymatic  
543 activity in HepaRG cells using UPLC-MS/MS. Anal Biochem **535**, 47-55.

544 Nepali, K., Lee, H.Y., Liou, J.P., 2019. Nitro-Group-Containing Drugs. J Med Chem **62**, 2851-2893.

545 Ramaiahgari, S.C., Auerbach, S.S., Saddler, T.O., Rice, J.R., Dunlap, P.E., Sipes, N.S., DeVito, M.J.,  
546 Shah, R.R., Bushel, P.R., Merrick, B.A., Paules, R.S., Ferguson, S.S., 2019. The Power of  
547 Resolution: Contextualized Understanding of Biological Responses to Liver Injury Chemicals  
548 using High-throughput Transcriptomics and Benchmark Concentration Modeling. Toxicol Sci.  
549 Re, J.L., De Meo, M.P., Laget, M., Guiraud, H., Castegnaro, M., Vanelle, P., Dumenil, G., 1997.  
550 Evaluation of the genotoxic activity of metronidazole and dimetridazole in human lymphocytes  
551 by the comet assay. Mutat Res **375**, 147-155.

552 Van den Eede, N., Cuykx, M., Rodrigues, R.M., Laukens, K., Neels, H., Covaci, A., Vanhaecke, T.,  
553 2015. Metabolomics analysis of the toxicity pathways of triphenyl phosphate in HepaRG cells  
554 and comparison to oxidative stress mechanisms caused by acetaminophen. Toxicol In Vitro **29**,  
555 2045-2054.

556 Zhang, L., Rylott, E.L., Bruce, N.C., Strand, S.E., 2019. Genetic modification of western wheatgrass  
557 (*Pascopyrum smithii*) for the phytoremediation of RDX and TNT. Planta **249**, 1007-1015.  
558  
559

560 OECD - Guidelines for the Testing of Chemicals, Section 4. [https://www.oecd-  
561 ilibrary.org/environment/oecd-guidelines-for-the-testing-of-chemicals-section-4-health-  
562 effects\\_20745788](https://www.oecd-ilibrary.org/environment/oecd-guidelines-for-the-testing-of-chemicals-section-4-health-effects_20745788). (accessed 15 October 2018).

563

564 OECD - Guidance Document on Good In Vitro Method Practices (GIVIMP).

565 [http://www.oecd.org/fr/env/ess/guidance-document-on-good-in-vitro-method-practices-givimp-](http://www.oecd.org/fr/env/ess/guidance-document-on-good-in-vitro-method-practices-givimp-9789264304796-en.htm)

566 [9789264304796-en.htm](http://www.oecd.org/fr/env/ess/guidance-document-on-good-in-vitro-method-practices-givimp-9789264304796-en.htm). (accessed 5 April 2019).

567

568

569 **Figures and Tables**

570 **Fig. 1** Effect of nitropyrazole-derived HEDMs on DNA repair mechanisms of differentiated HepaRG cells. **a** Gene analysis  
571 of DNA damage pathways by RNASeq following the incubation of differentiated HepaRG cells with 1 mM 1-nitropyrazole  
572 (1-NP), 1 mM 3-nitropyrazole (3-NP), 0.05 mM 1,3-dinitropyrazole (1,3-DNP), 1 mM 3,5-dinitropyrazole (3,5-DNP),  
573 0.250 mM 3,4,5-trinitropyrazole (3,4,5-TNP), 1 mM 4-nitropyrazole (4-NP) or 1 mM 1-methyl 4-nitropyrazole (1-Met-4-  
574 NP) for 24 h. Results are expressed in log<sub>2</sub> fold change and assigned a blue (decrease in expression) or red (increase in  
575 expression) color. The heat map was obtained with the XLSstat software, and the data shown represent three independent  
576 experiments. **b** Overlay of flow cytometry results for H2AX and  $\gamma$ H2AX foci quantification for HepaRG cells treated as  
577 in (a). Each nitropyrazole is compared cells treated with its relevant vehicle. 20  $\mu$ M doxorubicin was used as a positive  
578 control. Flow cytometry plots are representative of 2 independent experiments. *MeOH* methanol, *ACN* acetonitrile, *DMSO*  
579 dimethyl sulfoxide

580

581 **Fig. 2** Evaluation of the effect of nitropyrazole-derived HEDMs 1 mM 1-nitropyrazole (1-NP), 1 mM 3-nitropyrazole (3-  
582 NP), 0.05 mM 1,3-dinitropyrazole (1,3-DNP), 1 mM 3,5-dinitropyrazole (3,5-DNP), 0.250 mM 3,4,5-trinitropyrazole  
583 (3,4,5-TNP), 1 mM 4-nitropyrazole (4-NP) or 1 mM 1-methyl 4-nitropyrazole (1-Met-4-NP) on cellular stress in  
584 differentiated HepaRG cells. **a** Transcriptomic analysis by RNASeq of genes implicated in the DNA damage pathway.  
585 Differentiated HepaRG were treated with nitropyrazole-derived HEDMs for 24 h. Results are expressed in log<sub>2</sub> fold change  
586 and data were assigned a blue (decrease in expression) or red (increase in expression) color. The heat map was obtained  
587 with the XLSstat software, and the data represent three independent experiments. **b** Reactive oxygen species (ROS) were  
588 measured using the CM-H<sub>2</sub>DCFDA probe in differentiated HepaRG cells incubated for 30 min with a positive control (1  
589 mM H<sub>2</sub>O<sub>2</sub>), and either 90 min with equivalent amounts of vehicles (negative control), or nitropyrazole-derived HEDMs as  
590 in (a). Total ROS production was quantified by flow cytometry as the mean fluorescence intensity of cells. Data are  
591 expressed as mean  $\pm$  S.E.M. of at least two independent experiments. **c** Quantification of NO reactive derivatives (RNS)  
592 was performed through the measurement of intracellular DAF-FM accumulation by flow cytometry in differentiated  
593 HepaRG cells treated for 60 min with nitropyrazole-derived HEDMs as in (a). Data are expressed as the percentage increase  
594 (mean  $\pm$  S.E.M.) in mean fluorescence intensity of total NO reactive derivatives (RNS) for at least two independent  
595 experiments. Control cells were incubated with equivalent amounts of vehicles. Statistical analysis (Mann-Whitney) was  
596 conducted using GraphPad, NS not significant; \*  $P < 0.05$ ; \*\*  $P < 0.01$  *ACN* acetonitrile, *DMSO* dimethyl sulfoxide

597

598 **Fig. 3** Effect of Nitropyrazole-derived HEDMs 1 mM 1-nitropyrazole (1-NP), 1 mM 3-nitropyrazole (3-NP), 0.05 mM  
599 1,3-dinitropyrazole (1,3-DNP), 1 mM 3,5-dinitropyrazole (3,5-DNP), 0.250 mM 3,4,5-trinitropyrazole (3,4,5-TNP), 1 mM  
600 4-nitropyrazole (4-NP) or 1 mM 1-methyl 4-nitropyrazole (1-Met-4-NP) on metabolomics of differentiated HepaRG cells,  
601 assessed by (a) gene analysis (RNASeq) after 24 h incubation. Results are represented in log<sub>2</sub> fold change and assigned a  
602 blue (decrease in expression) or red (increase in expression) color. The heat map was obtained with the XLSstat software,  
603 and the data represent three independent experiments. **b** Targeted metabolites were also quantified in HepaRG cells treated  
604 for 36 h as in (a) by LC-HRMS. Data are expressed as mean ± S.E.M. of at least three independent experiments.

605

606 **Tables:**

607 **Table 1** Overview of the different nitropyrazole-derived HEDMs used throughout this study, as well as their corresponding  
608 concentration, chemical structure and molecular weight. *ACN* acetonitrile, *DMSO* dimethyl sulfoxide

609

610 **Table 2** Cellular cytotoxicity of various concentrations of nitropyrazole-derived HEDMs measured using either an MTT  
611 assay (cell viability) or the xCELLigence technology (cell proliferation). **a** The first three columns indicate the half  
612 maximum inhibitory concentration (IC<sub>50</sub>) obtained following MTT assays in the rodent CHO-K1, BALB/3T3 clone (A31),  
613 L5178T TK+/- (clone 3.7.2C) cells, after 72 h exposure to the indicated nitropyrazole-derived HEDMs (their respective  
614 vehicles are indicated in brackets). Data are expressed as mean ± S.D (N > 3 independent experiments). The last column  
615 presents xCELLigence results obtained in the only rodent cell line that grew in the specific xCELLigence chambers, namely  
616 the CHO-K1 cells. This shows the percentage of viable cells (compared to the vehicle condition) after incubation with  
617 nitropyrazole-derived molecules, the initial concentrations of which were obtained through the MTT assays. Statistical  
618 analysis (One-way ANOVA) was conducted using GraphPad, NS not significant; \* *P* < 0.05; \*\* *P* < 0.01. **b** The first two  
619 columns present MTT assays in human PSF04062 and CRC05 fibroblast cells after 72 h exposure to the indicated  
620 nitropyrazole molecules. Data are expressed as mean ± S.D (N > 2 independent experiments), ND not determined. The last  
621 column shows results obtained with the xCELLigence technology in human PSF04062 cells. Data are expressed as  
622 percentage of viable cells compared to vehicle (untreated) conditions. Statistical analysis (One-way ANOVA) was  
623 conducted using GraphPad, NS not significant; \* *P* < 0.05; \*\* *P* < 0.01.

624 *ACN* acetonitrile, *DMSO* dimethyl sulfoxide, *NP* nitropyrazole, *DNP* dinitropyrazole, *TNP* trinitropyrazole, *M* methyl

625

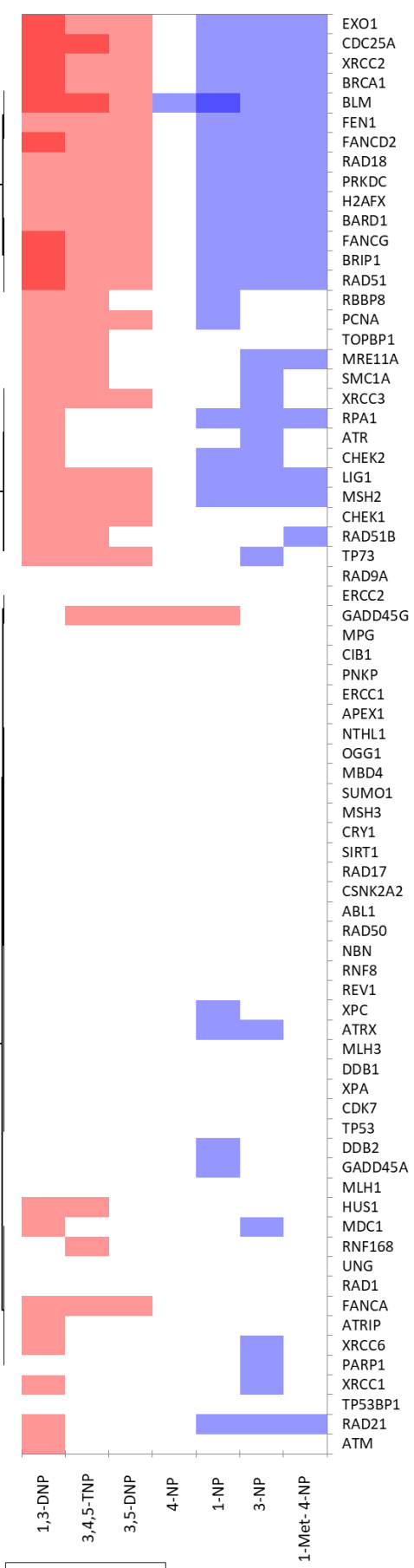
626

627 **Table 3** Cytotoxic effects of various concentrations of nitropyrazole-derived HEDMs on proliferative and differentiated  
628 HepaRG cells. The first part of the table indicates the half maximum inhibitory concentration ( $IC_{50}$ ) of the molecules  
629 incubated with proliferative or differentiated HepaRG cells for 72 h, obtained by MTT assays. All data represent the mean  
630  $\pm$  S.D. of at least three separate experiments. The second part of the table reports the effect of these molecules on the cell  
631 cycle of proliferative HepaRG cells, measured via a flow cytometry analysis of BrdU incorporation into cells over 24 h.  
632 Data are expressed as mean  $\pm$  S.D. of at least two independent experiments. Statistical significance (One-way ANOVA)  
633 was obtained using the GraphPad software. *NS* not significant; \*  $P < 0.05$ ; \*\*  $P < 0.01$ ; \*\*\*  $P < 0.001$ ; \*\*\*\*  $P < 0.0001$ .  
634 *ACN* acetonitrile, *DMSO* dimethyl sulfoxide, *NP* nitropyrazole, *DNP* dinitropyrazole, *TNP* trinitropyrazole, *M* methyl  
635  
636

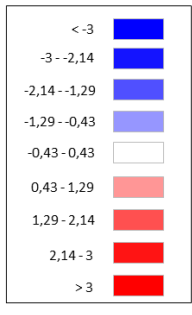
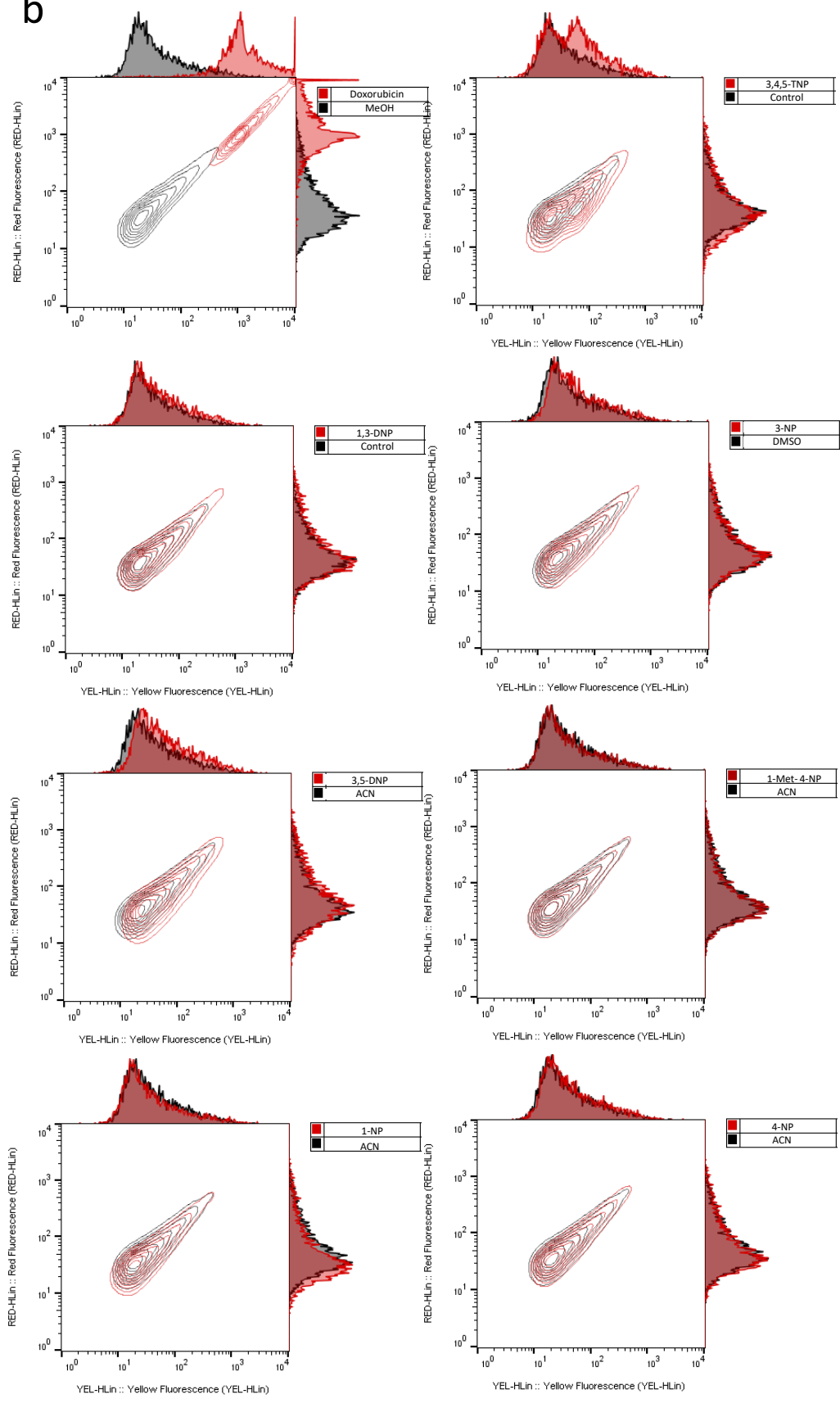
637 **Table 4** Variation in the expression of transcripts involved in cell death mechanisms in differentiated HepaRG cells treated  
638 for 24 h with Nitropyrazole-derived HEDMs at the following concentrations 1 mM 1-nitropyrazole (1-NP), 1 mM 3-  
639 nitropyrazole (3-NP), 0.05 mM 1,3-dinitropyrazole (1,3-DNP), 1 mM 3,5-dinitropyrazole (3,5-DNP), 0.250 mM 3,4,5-  
640 trinitropyrazole (3,4,5-TNP), 1 mM 4-nitropyrazole (4-NP) or 1 mM 1-methyl 4-nitropyrazole (1-Met-4-NP). This table  
641 presents the list of genes studied for the necrosis, the autophagy and the senescence pathways by RNAseq. Only genes  
642 with at least 50% of variation, either an increase ( $\uparrow$ ) or a decrease ( $\downarrow$ ) are represented for each molecule. The log 2 fold  
643 changes were calculated using the vehicles as controls. The data represent three independent experiments.  
644

645 **Table 5** Proportion of apoptotic cells (early and late stage apoptosis) following the incubation of differentiated HepaRG  
646 cells with nitropyrazole-derived HEDMs for 24 h and 72 h. The final assay concentrations were 1 mM 1-nitropyrazole (1-  
647 NP), 1 mM 3-nitropyrazole (3-NP), 0.05 mM 1,3-dinitropyrazole (1,3-DNP), 1 mM 3,5-dinitropyrazole (3,5-DNP), 0.250  
648 mM 3,4,5-trinitropyrazole (3,4,5-TNP), 1 mM 4-nitropyrazole (4-NP) or 1 mM 1-methyl 4-nitropyrazole (1-Met-4-NP).  
649 These results were obtained with the Muse® Annexin V and Dead Cell Assay Kit. Data are expressed as mean  $\pm$  S.E.M. of  
650 at least two independent experiments. Statistical analysis (Two-way ANOVA) was conducted using the GraphPad  
651 software. *NS* not significant, \*  $P < 0.05$ .  
652  
653

a



b





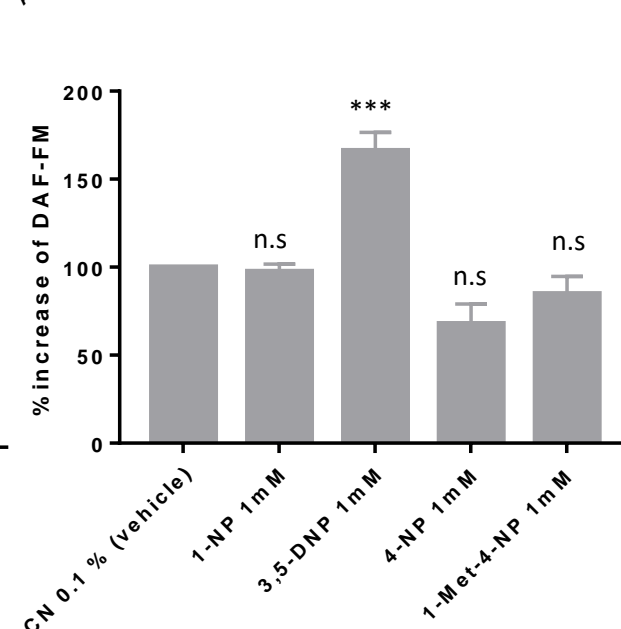
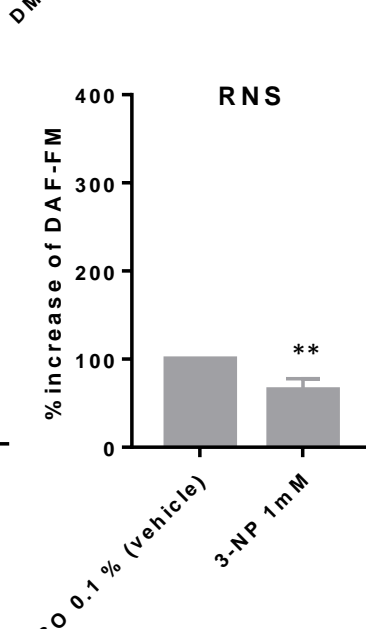
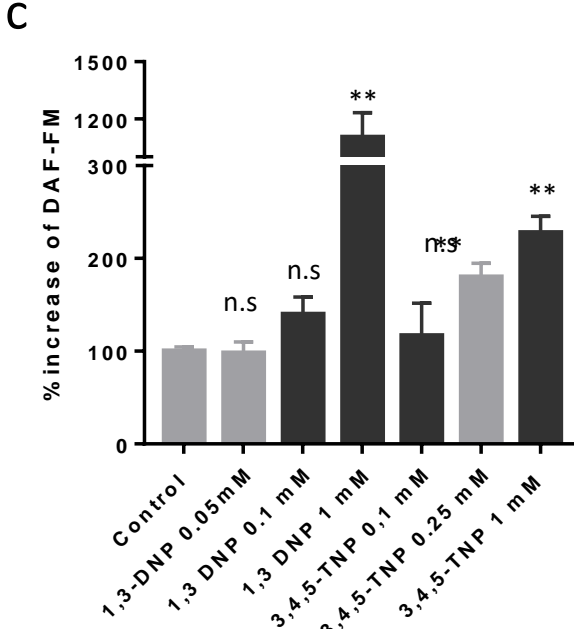
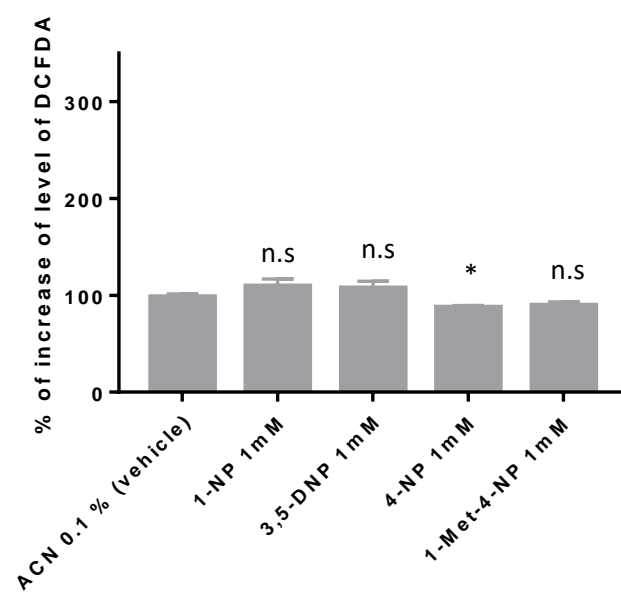
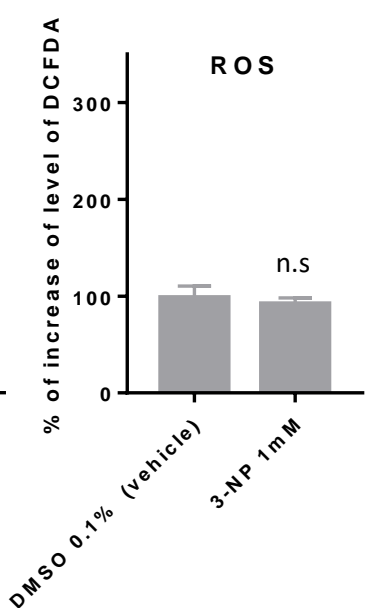
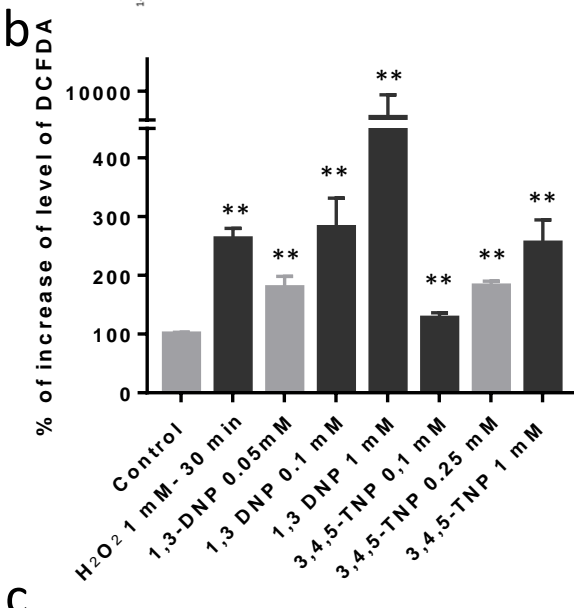
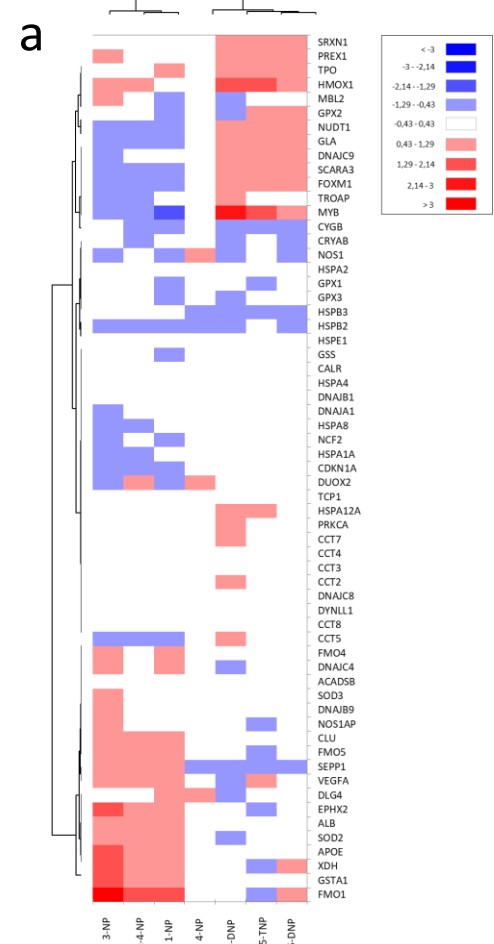
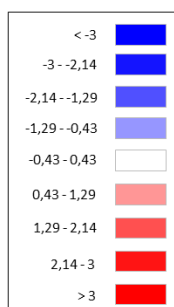
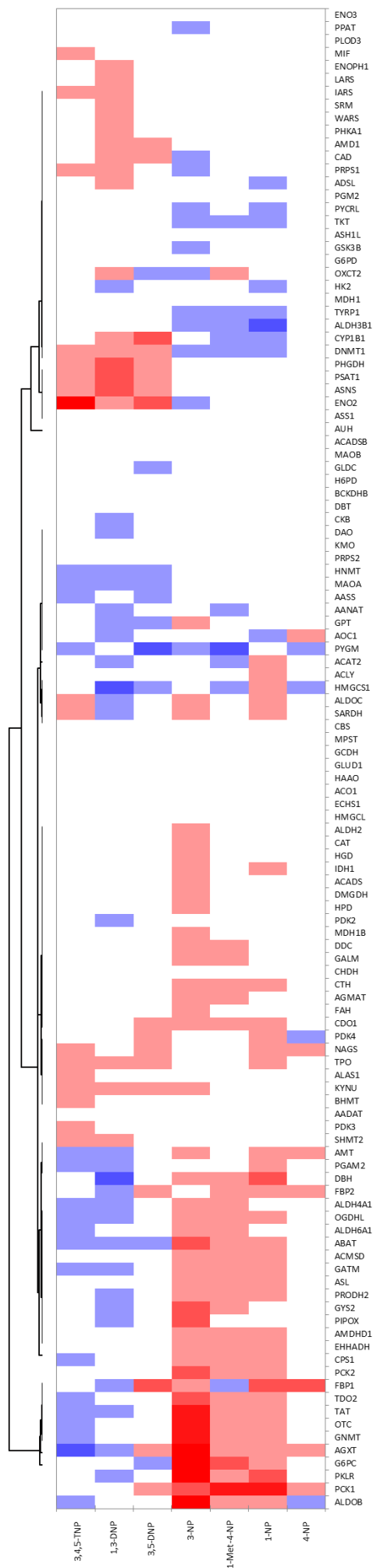
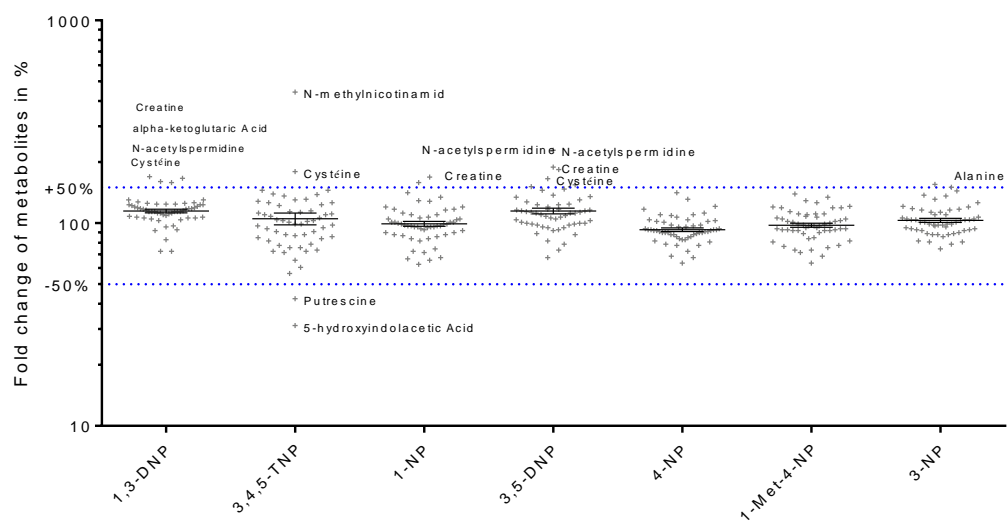


Figure 2

a



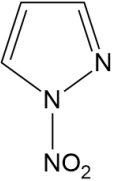
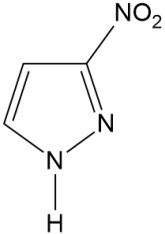
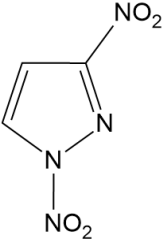
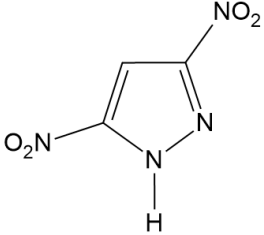
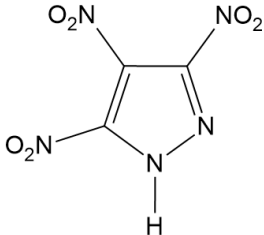
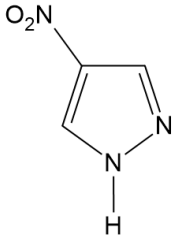
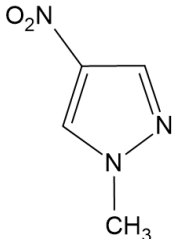
b



**Molecules studied :** alpha-ketoglutaric Acid, Acetylcholine, Aconitic Acid, Aspartic Acid, Citric Acid, Fumaric Acid, Glutamic Acid, Isocitric Acid, Malic Acid, N-acetylneuraminic Acid, Pantothenic Acid, Pyroglutamic Acid, Succinic Acid, 2-Methyl Hipuric Acid, 2-oxoglutaric Acid, 4-coumaric Acid, 5-hydroxyindolacetic Acid, Adenosine, Alanine, Arginine, Asparagine, Biotine, Choline, Choline phosphate, Creatine, Cystéine, Fructose-6-Phosphate, 3-Aminoisobutyric Acid, Glutamine, Reduced Glutathione, Glycero-3-phosphocholine, Histidine, Inosine, Isoleucine, Leucine, Lysine, Methionine, N-acetylmethionine, N-acetylspermidine, NAD, Nicotinamide, N-methylnicotinamid, O-propanoylcarnitine, Ornithine, Phenylalanine, Proline, Putrescine, S-Adenosyl-L-Homocysteine, S-Adenosyl Methionine, Serine, Spermidine, Spermine, Threonine, Tyrosine, UDP-Glucose, and Valine.

Figure 3

**Table 1.** Overview of the different nitroimidazole-derived HEDMs used throughout this study

Name	1-Nitroimidazole (1-NP)	3-Nitroimidazole (3-NP)	1,3-Dinitroimidazole (1,3-DNP)	3,5-Dinitroimidazole (3,5-DNP)	3,4,5-Trinitroimidazole (3,4,5-TNP)	4-Nitroimidazole (4-NP)	1Methyl 4-Nitroimidazole (1-Met-4-NP)
Solvent	ACN	DMSO	Water	ACN	Water	ACN	ACN
Initial concentration	1 M	1 M	100 mM	770 mM	1 M	1 M	1 M
Structure							
Molecular weight (g/mol)	113.07	113.07	158.07	158.07	203.00	113.07	127.1

**Table 2a.** Cellular cytotoxicity of various concentrations of nitroprazole-derived HEDMs measured using either an MTT assay (cell viability) or the xCELLigence technology (cell proliferation).

	BALB/3T3 clone (A31)	L5178Y TK +/- clone (3.7.2C)	CHO-K1			
	MTT IC <sub>50</sub>	MTT IC <sub>50</sub>	MTT IC <sub>50</sub>	x-CELLigence		
Molecules (vehicle)	mM	mM	mM	mM	% of confluence of treated condition ( compared to the confluence of the control)	<i>P-value</i>
<b>1-NP (ACN 0.1 %)</b>	0.945 ± 0.154	1.690 ± 0.370	0.313 ± 0.090	1.000	97% ± 9%	NS
<b>3-NP (DMSO 0.1 %)</b>	1.230 ± 0.260	> 10	3.570 ± 0.850	1.250	35% ± 7%	*
				0.625	107% ± 10%	NS
<b>1,3-DNP (water)</b>	0.007 ± 0.003	0.006 ± 0.001	0.002 ± 0.001	0.007	7% ± 8%	**
				0.004	64% ± 15%	NS
				0.001	100% ± 20%	NS
				0.001	100% ± 20%	NS
<b>3,5-DNP (ACN 0.1 %)</b>	1.020 ± 0.430	1.100 ± 0.830	0.886 ± 0.015	1.020	52% ± 17%	NS
				0.500	97% ± 27%	NS
<b>3,4,5-TNP (water)</b>	0.038 ± 0.007	0.010 ± 0.001	0.034 ± 0.002	0.038	57% ± 3%	NS
				0.019	93% ± 33%	NS
<b>4-NP (ACN 0.1 %)</b>	3.000 ± 0.530	> 10	3.350 ± 0.860	10.000	8% ± 0%	*
				5.000	34% ± 5%	NS
				2.500	62% ± 8%	NS
				1.250	86% ± 19%	NS
				0.625	100% ± 2%	NS
<b>1-Met-4-NP (ACN 0.1 %)</b>	8.050 ± 0.750	> 10	> 10	10.000	28% ± 1%	NS
				5.000	65% ± 2%	NS
				2.500	68% ± 7%	NS
				1.250	115% ± 30%	NS

**Table 2b.** Cellular cytotoxicity of various concentrations of nitropyrazole-derived HEDMs measured using either an MTT assay (cell viability) or the xCELLigence technology (cell proliferation).

	Human Fibroblast CRC05	Human Fibroblast PFS 04062			
	MTT IC <sub>50</sub>	MTT IC <sub>50</sub>	x-CELLigence		
Molecules (vehicle)	mM	mM	mM	% of confluence of treated condition (compared to the confluence of the control)	<i>P-value</i>
1-NP (ACN 0.1 %)	3.500	5.000 ± 0.770	5.7	84% ± 4%	NS
3-NP (DMSO 0.1 %)	> 10	> 10	10	30% ± 8%	*
			5	86% ± 25%	NS
			2.5	92% ± 16%	NS
			1.25	124% ± 0%	NS
1,3-DNP (water)	0.014	0.028 ± 0.006	0.019	0% ± 1%	**
			0.009	11% ± 3%	**
			0.004	55% ± 2%	NS
			0.002	105% ± 25%	NS
3,5-DNP (ACN 0.1 %)	> 10	6.250 ± 1.250	10.000	0% ± 4%	**
			5.000	8% ± 2%	**
			2.500	77% ± 2%	NS
			1.250	99% ± 0%	NS
3,4,5-TNP (water)	0.2	0.250 ± 0.020	0.250	2% ± 2%	**
			0.125	72% ± 7%	NS
			0.065	96% ± 11%	NS
			0.035	94% ± 21%	NS
4-NP (ACN 0.1 %)	ND	>10	5.000	47% ± 16%	NS
			2.500	49% ± 4%	NS
			1.250	59% ± 3%	NS
			0.625	78% ± 6%	NS
1-Met-4-NP (ACN 0.1 %)	ND	>10	5.000	70% ± 7%	NS
			2.500	78% ± 12%	NS
			1.250	72% ± 8%	NS
			0.625	106% ± 17%	NS

IC<sub>50</sub> : the concentration for which only there is 50 % of viable cells compared to the non-treated conditions at 72H. ND: not determined

<b>Table 3a.</b> Cytotoxic effects of various concentrations of nitroprazole-derived HEDMs on proliferative and differentiated HepaRG cells.							
n=3-4	1-NP (ACN)	3-NP (DMSO)	1,3-DNP (water)	3,5-DNP (ACN)	3,4,5-TNP (water)	4-NP (ACN)	1-Met-4-NP (ACN)
<b>Proliferative cells</b>	0.850 ± 0.250 mM	> 10 mM	0.014 ± 0.003 mM	1.560 ± 0.510 mM	0.264 ± 0.040 mM	> 10 mM	> 10 mM
<b>Differentiated cells</b>	> 10 mM	8.300 ± 1.030 mM	0.105 ± 0.001 mM	5.700 ± 0.190 mM	0.205 ± 0.020 mM	> 10 mM	> 10 mM

<b>Table 3b.</b> Effect of the nitroprazole-derived HEDMs on the cell cycle of proliferative HepaRG cells, measured via a flow cytometry analysis of BrdU incorporation into cells over 24 h							
	Concentration	S %	P-value	G2M %	P-value	G1 %	P-value
<b>Water</b>		18.4 ± 0.0		7.1 ± 0.0		71.5 ± 0.0	
<b>1,3-DNP</b>	0.05 mM	22.9 ± 1.5	*	11.7 ± 0.0	**	60.3 ± 0.3	****
<b>3,4,5-TNP</b>	0.25 mM	27.9 ± 1.2	****	11.8 ± 0.2	***	55.1 ± 1.3	****
<b>DMSO 0.1%</b>		14.7 ± 1.6		6.0 ± 0.1		75.9 ± 1.8	
<b>3-NP</b>	1.00 mM	15.9 ± 0.9	NS	8.4 ± 1.5	NS	71.5 ± 1.5	NS
<b>ACN 0.1%</b>		17.1 ± 1.1		5.6 ± 0.5		74.8 ± 0.7	
<b>1-NP</b>	1.00 mM	6.8 ± 0.9	****	8.6 ± 0.2	NS	77.2 ± 0.9	NS
<b>3,5-DNP</b>	1.00 mM	23.4 ± 0.8	**	8.7 ± 1.9	*	63.4 ± 2.3	****
<b>4-NP</b>	1.00 mM	15.4 ± 1.0	NS	7.6 ± 1.4	NS	73.8 ± 1.6	NS
<b>1-Met-4-NP</b>	1.00 mM	14.5 ± 0.4	NS	10.0 ± 0.3	**	72.6 ± 0.5	NS

Each condition was in duplicate, and at least three independent experiments were carried out.

Table 4. Variation in the expression of transcripts involved in cell death mechanisms in differentiated HepaRG cells treated for 24 h with nitropyrazole-derived HEDMs									
	Unchanged transcriptomics expression level of these genes	Gene variation (log <sub>2</sub> FdC)							
		3,4,5-TNP	1,3-DNP	3,5-DNP	3-NP	1-Met-4-NP	1-NP	4-NP	
<b>NECROSIS</b>	ATP6V1G2, BMF, C1orf159, CCDC103, COMMD4, CYLD, DEFB1, DENND4A, DPYSL4, EIF5B, GALNT5, GRB2, HSPBAP1, PARP2, PVR, SPATA2, TMEM57, TXNL4B		PARP2 (↑)					GALTN5 (↓)	
<b>AUTOPHAGY</b>	AMBRA1, APP, ATG10, ATG12, ATG16L1, ATG16L2, ATG3, ATG4A, ATG4B, ATG4C, ATG4D, ATG5, ATG7, ATG9A, CLN3, CTSB, CXCR4, DRAM1, GABARAP, GABARAPL1, GABARAPL2, HDAC6, HSP90AA1, IGF1, LAMP1, MAP1LC3B, NPC1, PIK3R4, RAB24, RGS19, TMEM74, ULK1, UVRAG, WIP1		CXCR4 (↓) TMEM74 (↑)				CXCR4 (↑) IGF1 (↑)	CXCR4 (↑) IGF1 (↑)	IGF1 (↓)
<b>SENESCENCE</b>	BMI1, CD44, CDKN2C, CDKN2D, CITED2, COL1A1, COL3A1, CREG1, E2F3, EGR1, ETS1, ETS2, FN1, GLB1, HRAS, ID1, IGFBP3, IGFBP5, IGFBP7, ING1, IRF3, IRF5, IRF7, MAP2K1, MAP2K3, MAP2K6, MAPK14, MORC3, NOX4, PLAU, PRKCD, SERPINE1, SPARC, TERF2, TGFB1I1, THBS1, TWIST1, VIM	COL3A1 (↓) IGFBP3 (↑) SERPINE1 (↑)	IGFBP5 (↓) SERPINE1 (↑) TGFB1I1 (↓)	IGFBP5 (↓) SERPINE1 (↑)	SPARC (↑)	NOX4 (↑) PLAU (↓) VIM (↓)	COL1A1 (↑) IRF7 (↑) NOX4 (↑) VIM (↓)		

The increase with at least 50% is represented by (↑)

The decrease with at least 50% is represented by (↓)

24H exposure of differentiated Hepa-RG Cells

Exposure to no toxic concentrations of pyrazol

The fold changes are calculated with the vehicles control treated under the same experimental conditions

It is presented the mean of 3 independent experiments

**Table 5.** Proportion of apoptotic cells (early and late stage apoptosis) following the incubation of differentiated HepaRG cells with nitroprazole-derived HEDMs for 24 h and 72 h.

Treatment	24 H								72 H							
	Dead cells	<i>p</i> -value	Late apoptotics cells	<i>p</i> -value	Early apoptotics cells	<i>p</i> -value	Live cells	<i>p</i> -value	Dead cells	<i>p</i> -value	Late apoptotics cells	<i>p</i> -value	Early apoptotics cells	<i>p</i> -value	Live cells	<i>p</i> -value
Water	6.49 ± 0.16		2.30 ± 0.17		0.91 ± 0.10		90.60 ± 0.50		8.40 ± 1.70		1.09 ± 0.89		0.23 ± 0.13		90.35 ± 2.65	
1,3-DNP 0.05 mM	6.60 ± 0.17	NS	1.45 ± 0.05	NS	0.43 ± 0.04	NS	91.70 ± 0.10	NS	9.76 ± 2.14	NS	0.94 ± 0.19	NS	0.18 ± 0.04	NS	89.25 ± 2.25	NS
3,4,5-TNP 0.25 mM	5.60 ± 0.19	NS	1.23 ± 0.26	NS	0.26 ± 0.10	NS	93.05 ± 0.25	NS	11.05 ± 0.05	NS	1.66 ± 0.12	NS	0.19 ± 0.01	NS	87.30 ± 0.10	NS
DMSO 0.1 %	6.62 ± 0.26		2.23 ± 0.10		0.91 ± 0.02		90.55 ± 0.45		10.63 ± 0.97		1.52 ± 0.01		0.24 ± 0.15		87.85 ± 0.85	
3-NP 1 mM	6.89 ± 1.06	NS	2.15 ± 0.23	NS	0.80 ± 0.17	NS	90.50 ± 1.50	NS	10.23 ± 0.47	NS	1.67 ± 0.12	NS	0.23 ± 0.01	NS	88.05 ± 0.65	NS
ACN 0.1 %	5.92 ± 0.12		1.69 ± 0.02		0.61 ± 0.04		92.05 ± 0.15		10.49 ± 1.02		1.44 ± 0.32		0.20 ± 0.06		88.00 ± 0.70	
1-NP 1 mM	7.65 ± 0.28	*	1.44 ± 0.28	NS	0.51 ± 0.02	NS	90.70 ± 0.60	NS	11.00 ± 0.30	NS	2.07 ± 0.04	NS	0.31 ± 0.01	NS	86.90 ± 0.30	NS
3,5-DNP 1mM	5.47 ± 0.24	NS	1.86 ± 0.02	NS	0.70 ± 0.01	NS	92.25 ± 0.15	NS	13.15 ± 0.25	NS	2.69 ± 0.65	NS	0.31 ± 0.06	NS	84.05 ± 0.95	*
4-NP 1mM	6.09 ± 0.15	NS	1.32 ± 0.45	NS	0.51 ± 0.08	NS	92.30 ± 0.30		11.50 ± 0.40	NS	1.37 ± 0.02	NS	0.31 ± 0.06	NS	87.10 ± 0.40	NS
1-Met-4-NP 1mM	5.58 ± 0.04	NS	1.50 ± 0.18	NS	0.28 ± 0.04	NS	92.80 ± 0.20	NS	9.64 ± 0.66	NS	1.54 ± 0.09	NS	0.37 ± 0.08	NS	88.60 ± 0.60	NS